Spatio-temporal patterns of snow in the Catalan Pyrenees (NE Iberia)

Josep Bonsoms [1], Sergi Gonzalez [2], Marc Prohom [3], Pere Esteban [3],
Ferran Salvador-Franch [1]; López-Moreno, J.I. [4]& Marc Oliva [1]

[1] Department of Geography, Universitat de Barcelona, Barcelona, Catalonia, Spain
[2] Antarctic Group, Spanish Meteorological Agency (AEMET), Barcelona, Catalonia, Spain
[3] Meteorological Service of Catalonia, Barcelona, Catalonia, Spain
[4] Instituto Pirenaico de Ecología (IPE-CSIC), Campus de Aula Dei, Zaragoza, Spain

*Corresponding author: Josep Bonsoms
Email: josepbonsoms5@gmail.com
Telephone number: +34 655 36 49 42
Department of Geography, Universitat de Barcelona
Montalegre 6-8, 3r floor, 08001 - Barcelona

Abstract: In a warmer climate, significant variations in the snow regime are expected. Thus, it is crucial to better understand present-day snow cover regime, its duration and thickness, in order to anticipate future changes. This work presents the first characterization of snow patterns in the Catalan Pyrenees based on eleven snow stations located in high elevation areas (>2000 m). Here, we examine spatio-temporal evolution of the daily snow depth and new snow height (HN) since the earliest 2000s to 2020. In addition, we analyze the different synoptic patterns that cause HN events in the study area as well as the low frequency climate modes on the different stages of the snow season. Our results show evidence that the measured snow amount differs considerably between the western and the eastern Catalan Pyrenees independently of the considered elevation. While the eastern part has an average seasonal cumulative HN of 278 cm, the western sector gets almost twice (433 cm). Nonetheless, the onset of the snow melting does not show substantial differences, being primarily ruled by the elevation in both areas. The longest snow records (Núria, 1971 m) point to an increase of HN from 1985 to 2020, a trend which is also observed in most stations from 2000 to 2020. Nevertheless, some stations of the western fringe record negative trends associated with the low frequency variability of the Western Mediterranean Oscillation (WeMO). Results also indicate that the NW Atlantic low-pressure systems are the circulation weather types that provide more abundant HN in the majority of snow stations. The Atlantic advections are more frequent in autumn and winter, whilst the Mediterranean advections provide more intense and recurrent HN in spring. The atmospheric circulation is basically ruled by the East Atlantic/West Russia and the WeMO teleconnection patterns.

Key words: Pyrenees; Snow; Climate variability; Circulation types; Teleconnection patterns.

1. Introduction

Over the last decades, snowfall trends have shown a different pattern of change depending on the latitude, distance to the sea as well as the elevation of the measuring sites. Whereas an overall decline of snow cover has been detected for the Northern Hemisphere (Brown and Robinson, 2011; Notarnicola, 2020), in mountain areas is frequent to find a decrease of new snow height (HN) and snow depth (SD) at the lowest elevations of most mid-latitude high mountain ranges, while the HN and SD trends at high elevations have not shown significant trends (IPCC, 2019). Snow projections for the future under different scenarios agree to indicate a generalized decline of snowpack for most mountains of the world; and mountains located in

the Mediterranean basin have been pointed out to be particularly sensitive to climate warming (López-Moreno et al., 2020a).

The Pyrenees is one of the most important mountain areas of the Mediterranean basin in both extension and elevation. This mountain bridge stretching ca. 450 km between the Atlantic and the Mediterranean Sea constitutes also the linkage between the Iberian Peninsula with the Eurasian continent, with peaks consistently above 2000 m a.s.l and exceeding 3000 m in the central part of the range. In the Pyrenees, the snow is abundant during the winter season and persists between 6-8 months at elevations above 2000 m (Oliva et al., 2016). The presence of the snow favours the existence of a wide range of socioeconomic activities. For instance, the snow tourism business established in this region guarantees the economic and demographic stabilization of the population settled in the area (López-Palomeque, 1996). Moreover, the snowfall stored as a snowpack is a water reservoir for several large cities located downstream. Beyond social aspects, snow is a natural element crucial for ecological processes (García-Ruiz et al., 2011; López-Moreno et al., 2017). Therefore, an accurate characterization of the temporal and spatial evolution of snow in the Pyrenees is needed to anticipate potential changes under the future warming scenario projected (TICCC, 2016).

Between 1961 and 2013, Buisan et al. (2014) detected a (non-statistically significant) decrease of winter snow days in the valley bottoms (ca. 1000 m) of the southern western Pyrenees. However, from 1981 to 2010 a (non-statistically significant) increase was observed for the same regions. López-Moreno et al. (2020b) pointed out a reduction of the SD and the snow cover days in the entire range for the last six decades (1958-2017). Both studies defined the reduction of the circulation types (CT) related to snowfall as the factor of the trends observed, together with the climate warming in the case of SD evolution. The CT supplying the most abundant solid precipitation during the winter season in the western and central Pyrenees correspond to N, W and especially NW advections (e.g., Esteban et al., 2005; López-Moreno et al., 2007). Nevertheless, N advections record less snow amounts moving into the eastern sectors of the Pyrenees. This was observed both at mid-low altitude areas (ca. 1000 m; Buisan et al., 2014) and also at higher elevations of the western and central Pyrenees (>1800 m; Navarro-Serrano et al., 2017). Similar patterns were also observed in other neighbouring mountain regions, such as the Swiss Alps, where the reduction of snowfall during winters from 1980 to 1990 was associated with more frequent than usual positive phases of the North Atlantic Oscillation (NAO; Beniston et al., 1997). The NAO has been also identified as one of the main teleconnection index to control the duration and magnitude of snowpack in mountains of the

Mediterranean basin, including those in the Iberia Peninsula (López-Moreno et al., 2011), but with noticeable differences even at short distances depending on the elevation and exposition to dominant air masses associated to NAO (Alonso-González, et al., 2020). Therefore, large-scale precipitation regime changes are linked with synoptic conditions variations, which in turn are linked by the interdecadal variability of the large-scale climate modes.

There are several studies that have analysed the snow characteristics and trends in the western and central Pyrenees, as well as works focusing on the CT that control the snow accumulation and the associated teleconnection patterns. However, *in-situ* snow observations of the high elevations areas (>2000 m) of the eastern strip remained unstudied to the date. With the purpose of filling this gap, this study will give address to the following objectives:

i) Carry out an accurate characterization of the snow regime at the high elevation areas of the Catalan Pyrenees.

ii) Determine the spatial and temporal variation of snow accumulation and the corresponding CT.

iii) Evaluate and quantify the influence over the snow records of several atmospheric modes of variability affecting the Western Mediterranean basin.

2. Study area

The Pyrenees constitutes a mountain range aligned W-E at latitudes 42-43ºN and longitudes between 2ºW and 3ºE. The highest peaks are located on the central part of the range (Aneto, 3,404 m asl) with lower peaks in the western and eastern fringes. This research focuses on the Catalan Pyrenees, placed between the central and the eastern parts of the mountain range. The majority of the automatic weather stations (AWS) analyzed are located on the southern slopes of the Pyrenees and drains to the Mediterranean Sea (Figure 1), except Sasseuva, Bonaigua and Certascan stations that drains to the Atlantic Ocean. Most of the valleys have an N-S route crossing different geological units from the axial core of the range towards the sedimentary depressions located in the lowlands. The complex configuration of the relief, together with its location between different climatic influences, determines a wide spectrum of topoclimates.

The Pyrenees are in the transition belt between subtropical and westerlies dynamics influenced by two contrasted water masses, the Atlantic Ocean and the Mediterranean Sea (Ramos et al., 2014). Meteorological conditions are governed by the position of the jet stream circulation

leading to a contrasted regime of precipitation between summer and winter. In summer, when the circulation of the jet stream displaces northwards, strong convective precipitation dominates, as a result of the buoyancy of the rising parcels produced by surface heating of the mountain slopes (Houze, 2012). In contrast, winter precipitation is characterized mainly by the interaction of mid-latitude frontal systems with the mountain range (Roe, 2005). Geographically, the western-central Pyrenees record high precipitation evenly distributed along the year, with strong influences of the Atlantic climate, and a well distributed precipitation along the year. In contrast, precipitation in the eastward Catalan Pyrenees sectors is less evenly distributed through the season, reaching maximums in summer and minimums in winter (Martín Vide et al., 2011). From November to May, the average precipitation above 2000 m is ca. 700 mm at the eastern Catalan Pyrenees and Pre-Pyrenees and around 900 mm at the axial zone of the Pyrenees (Lemus-Canovas et al., 2018). The northern slopes record higher amounts of precipitation than the southern ones, receiving also less solar radiation. In the valley bottoms, due to topographic effects, lesser precipitation is measured than at higher elevations, and also markedly thermal inversions are observed. Due to mountain configuration, some valleys within the axial Pyrenees and the Pre-Pyrenees, show an amplification of their continental characteristics. The mean annual air temperature (MAAT) is close to 4 ºC at 2000 m (1961 to 1990; SMC, 2008).

3. Data and methodology

3.1 Weather station data

Observational data was selected from 11 AWS located above 1970 m, and managed by the Meteorological Service of Catalonia (SMC). All stations provide data for a set of meteorological variables: air temperature, relative humidity, global solar radiation, precipitation, wind direction and velocity and SD, using for the latter an acoustic sensor. For this study daily data was used. The dataset covers a 17-year common period (2003-2020) for the whole network. Núria SD records were available since 1985 to 2020, and the whole dataset was only analyzed in section 4.1. No remarkable location changes were reported for any AWS, except for Ulldeter that was moved from a height of 2364 m to the current (2410 m) in 2011. The dataset analyzed was checked using a combination of automatic and visual quality filters: gross errors, temporal consistency, internal coherency, climatological coherency, spatial coherency, and a final visual inspection (SMC, 2011). Additionally, radar data was also used as a support. The vast majority of the AWS have data coverage of 99% of the daily snow records (Table 1). However, Espot weather station has a 7% of gaps of the total records. Most of the missing data occurred during the 2005 year. Finally, we grouped months as follows: October and November (ON) correspond

to autumn (September was excluded because of the lack of snow in that month); December, January and February (DJF) as winter; and March, April and May (MAM) as spring season.

3.2 Methodology

The HN was calculated by the difference between maximum SD of two consecutive days. This method has some limitations since the snowpack is subject to several processes such as sublimation, melting and redistribution. However, the HN provides confidential results, and has been performed for decades at national weather services (Buchmann et al., 2020), for snow research at the Alps (e.g., Marty et al., 2012; Scherrer et al., 2013) or at the Pyrenees (e.g., Salvador-Franch et al., 2014; 2016). We retained only the days when the difference was >=1 cm, in order to avoid sensor noise (Navarro-Serrano et al., 2017, and references therein). The inter-seasonal variability of the seasonal cumulative HN was analysed using the coefficient of variation (CV). The CV is calculated by the ratio between the standard deviation (Std. Dv) and the seasonal cumulative HN. The snow melting date was defined by the day when the snow peak was reached. Finally, a multiple linear regression and a Pearson's correlation were performed in order to identify the relevance of the geographical factors (elevation, latitude, longitude and distance to the seas) on the snow parameters analyzed.

The seasonal cumulative HN trends were conducted by Mann-Kendall trend test and Sen's slope, a non-parametric statistical technique broadly used in climatology to identify data trends (Kendall et al., 1948). It is based on the comparison with the actual value respect the last value, assuming a positive trend if it is higher and a negative if it is lower. The Mann-Kendall trend test was decided over another parametric trend test because of (i) the low interference with outliers, and (ii) it does not suppose any previous distribution of the data. The test has been performed with seasonal data for the 11 stations, with the objective to evaluate if there was a reduction or an increase of the variables analyzed within the time series studied. Finally, the trend was considered statistically confidential if it is significant at 5% level.

The CT classification was undertaken with the SynoptReg R package (Lemus-Canovas et al., 2019). This R routine reproduces a Principal Component Analysis (PCA) based on extreme scores method, described by Esteban et al. (2005; 2009). Using a S-mode matrix and with varimax rotation, the components retained, 4 in this case (86% of variance), derive in 8 potential CT. Later, the real cases were classified thanks to the higher and lower values of the scores and the multidimensional distances by K-means clustering method, obtaining the catalogue of CT. This methodology has been successfully applied in Andorra to analyze heavy snowfalls

(Esteban et al., 2005), and in the study area to characterize lightning activity (Pineda et al., 2010) or precipitation (Lemus-Canovas et al., 2018). The database used for obtain the CT was daily SLP and Geopotential Height at 500 hPa obtained from NCEP/NCAR Reanalysis 2 (Kalnay et al., 1996) for 30ºN-60ºN by 30 ºW-10ºE with 2.5º resolution, encompassing all days since 1999 to 2020.

For a proper interpretation of the association between (i) the seasonal cumulative HN at the study sites and (ii) the intrinsic climate variability at large atmospheric scale, a Pearson's correlation analysis was performed, together with a significance test. We based our analysis on the teleconnection patterns that role precipitation in the western Mediterranean defined by Trigo et al. (2006). These include: (i) the EA pattern with a north-south dipole over the North Atlantic Ocean; (ii) the EAWR with a positive phase with positive anomalies in Eurasia and negative in the North Caspian; (iii) the SCAND, with a positive phase circulation center over Scandinavia, and negative centers over western Europe; (iv) the AO and a regional subtype, the (v) NAO, based on the difference of sea-level pressure in Reykjavik (Iceland) and Ponta Delgada (Azores). We included also (vi) the WeMO teleconnection pattern, previously identified as a driver of precipitation in the eastern Iberia (Martin-Vide, et al., 2006). The WeMO was calculated by the difference of pressure between Padua (Italy) and San Fernando (Spain). Finally, (vii) the lagged effect of ENSO events on the Catalan Pyrenees was measured by the Southern Oscillation Index (SOI) based on the standardised surface pressure between Tahiti and Darwin. The link was investigated by the average values of the last autumn SOI and the seasonal cumulative HN recorded during MAM, following the methodology performed by Rodó et al. (1997). The EA, EAWR and SCAND monthly data were downloaded from the National Center for Atmospheric Research (NCAR; https://www.cpc.ncep.noaa.gov/data/teledoc/teleintros.html). The AO, NAO, WeMO and SOI teleconnection patterns the data was provided by the Climate Research Unit (CRU), University of East Anglia (https://crudata.uea.ac.uk/cru/data/pci.htm).

4. Results and discussion

An accurate analysis of the snow data allows the characterization of HN and SD of the Catalan Pyrenees, showing the spatial differences, trends as well as the inter-seasonal divergences. Subsequently, we examine the most recurrent and effective CTs in terms of snow accumulation for each snow station, as well as the teleconnection pattern ruling seasonal cumulative HN in the study zones.

4.1. HN and SD analysis

The average seasonal cumulative HN recorded in the Catalan Pyrenees totals 363 cm. The higher values were observed in the western sector (433 cm), with a maximum at Bonaigua (545 cm). On the contrary, the eastern corner recorded lesser amounts (278 cm), with the highest values reached at Ulldeter (349 cm). The minimum snow values were observed at Salòria (230 cm) and at Port del Comte (194 cm; Figure 2 and 5). Both stations are emplaced in open zones, exposed to severe winds (Table 2) that favour the snow accumulation or drift depending on the wind direction. Rather than elevation or distance to the sea, the high HN values showed a greather dependence with Latitude ($r = 0.74$), and Longitude ($r = -0.52$; Table 3). The HN days for a season increased also toward the N ($r = 0.84$ with Latitude) and decreased to the E ($r = -0.68$ with Longitude). Around 49 HN days for a season were recorded in the western sector, meanwhile 13 days per season less were observed in the eastern. The maximum HN days per season were recorded at Bonaigua (58 days), whilst the minimum was measured at Núria (34 days), which could be also attributable to its lower elevation (1971 m). Contrasted SD and HS values were observed between western and eastern Catalan Pyrenees sectors. However, the inter-seasonal variability of the seasonal cumulative HN showed fewer differences between stations. The lowest CV values were reached in the N western Catalan Pyrenees (CV < 28%), whereas the maximum values were observed at Port del Comte and Salòria (CV = 45% in both cases). No significant differences between areas where observed during heavy HN events (>P75), and practically the same HN amount was observed at the western (11 cm) compared with the eastern (10 cm).

Despite the existence of two very different patterns in the Catalan Pyrenees, the snow season practically lasts the same period at equal elevation. Nonetheless, the maximum monthly cumulative HN was reached on different months. The average autumn cumulative HN at the eastern Catalan Pyrenees was around 30 cm, which is practically the half amount that was recorded in the western area (> 60 cm). In the northern area of this sector, the highest average monthly cumulative HN was recorded in winter. For instance, during January, Sasseuva averages 70 cm and Bonaigua and Certascan more than 100 cm (Figure 3). In the eastern Catalan Pyrenees, the largest monthly HN accumulation occurs during the spring months. March is the snowiest month for most stations, including also Boí (100 cm) and Salòria (47 cm), whereas April is the snowiest month for Espot (68 cm), and the easternmost station, Ulldeter (55 cm). The monthly cumulative HN progressively decreases through May, where precipitation gradually turns into rainfall. HN in June is practically anecdotic (i.e., only 6 cm at Ulldeter).

The results exposed are in accordance with previous studies carried out at the eastern Catalan Pyrenees (Salvador-Franch et al., 2012; 2016); indeed, snowfall at La Molina (1700 m) placed among Cadí-Nord and Núria, totals practically the same (251 cm; Salvador-Franch et al., 2012) than the nearest snow stations examined in this work. In the same line, Núria station records almost the same average seasonal cumulative HN amount (283 cm) and frequency (34 days/season) between 1985 and 2013 (Salvador-Franch et al., 2016) than from 1985 to 2020. In the western Pyrenees, the seasonal snow accumulation exceeds 500 cm, with lower inter-seasonal variability (ca. 20-25%) than at the eastern Pyrenees and the largest snow accumulation phase during winter (Navarro-Serrano et al., 2017).

The average SD for a season recorded at the N western Catalan Pyrenees rounds the 80 cm, almost fourfold the values reached on the eastern strip (ca. 20 cm). Regardless of the elevation, the SD values decreases abruptly following an N-S and W-E gradient ($r > 0.60$ with Latitude and Longitude). From W to E, the snow accumulation peak rises until >150 cm in the western stations, with a maximum at Bonaigua station (>200 cm). A lesser amount is recorded at Espot (56 cm) or at Salòria (26 cm), and finally around 50 cm are recorded in the eastern sector. The contrasted average seasonal cumulative of HN and SD exposed between sectors is explained because of western Pyrenees creates a shelter from the prevailing winds, leading to a shadow effect on the eastern Pyrenees under Atlantic advections (Pepin et al., 2006).

The seasonal SD profile was divided in two stages (Figure 4). During the first one or accumulation phase, successive snow events accompanied by low temperatures favour the snowpack growth. Negative snow balance days can happen (i.e., during warm anticyclonic days or moist and rainy days), however, the snow thickness tends to increase up towards a snow peak where SD begins to decrease. The elevation level where the AWS is placed is the principal factor that determines the earlier or later onset of melting ($r = 0.53$ between the average date onset of snow melting and elevation) with no differences between the Catalan Pyrenees sectors. This threshold is different between stations and takes place within more than a month of delay when lower and higher AWS stations are compared. In fact, snow starts to diminish earlier in the lower stations like Núria (1971 m) during the first weeks of February whilst at the higher-up stations (Ulldeter, 2410 m or Boí, 2535 m) the melting phase takes place at the first and second week of April, respectively. At Cadí-Nord (2143 m), the snow peak takes place also in April. This is attributable to the characteristics where the AWS is emplaced, on the N aspect

(therefore, with low solar radiation values) and is sheltered from the advections due to topography.

Through the approximately twenty seasons examined, encompassing the earliest 2000 to 2020 for the majority of the weather stations and from 1985 to 2020 in case of Núria weather station, seasonal cumulative HN trends have experienced few changes. Changes in the major climatic variables that control the HN, namely temperature and precipitation play a different role to explain temporal evolution of the snowpack (Moran-Tejeda et al., 2013). In the first phase, López-Moreno (2005) quantified for the central Pyrenees that precipitation explains ca. 80% of the snow variation over 1600 m between December to March. In the later month, temperature modulates the snow/rain ratio and the speed of melting. Therefore, variation on HN at this elevation must be read as precipitation shifts with low influence of climate warming. Throughout the snow accumulation phase, a negative trend (Kendall's τ value around 0.2) has been observed in the northern stations of the western sector and at Ulldeter, where it extends along all seasons. This reduction of the seasonal cumulative HN occurred principally at spring and also autumn months determining the seasonal trend in these stations (Figure 5 and 6). Contrary, positive seasonal cumulative HN trends are found in the eastern sector, including also Espot and Salòria (Kendall's τ value around 0.2). In winter months, a general increase of seasonal cumulative HN has been measured and only Port del Comte and Ulldeter showed a negative trend. Except at Salòria, none trend was statistically significant, which is in agreement with the non-statistically significant SD trends observed on the Pyrenees starting after 1980 (López-Moreno et al., 2020b). In fact, precipitation trends are often dependent on the analysed time slices. If we focus on a broad spatial and temporal scope, precipitation trends in the Mediterranean region have not declined over the last 150 years, showing no clear signs of anthropogenic climate forcing (Peña-Angulo et al., 2020). In a shorter temporal period and focusing on valley bottoms (<1500 m) of the Spanish Pyrenees, winter precipitation decreased (non-statistically significant) from 1961 to 2014 (Buisan et al., 2016), driven by more recurrent positive phases of the NAO (López-Moreno, 2005). Nevertheless, at the same area, winter precipitation increased (non-statistically significant) from 1981 to 2010 which was linked with variations in the frequency of W CT (Buisan et al., 2016; López-Moreno et al., 2020). At higher elevations (ca. 1800 m) of the northern Pyrenees, between 1958 and 2008 an increase of precipitation during the winter season was observed (Maris et al., 2009), which was probably associated with the weak influence of the NAO index on the winter snowfall at this sector of the Pyrenees (Alonso-González et al., 2020). The W wind flows, in combination with a (non-statistically significant) negative trend of winter temperatures (El Kenawy et al., 2012; OPCC,

2019) triggered an increase of snow accumulation (Buisan et al., 2016). Indeed, the positive trend analysed which outsets in 1985 (Núria) is explained because 1980 and 1990 were dry and mild years in SW Europe, including the Swiss Alps driven by more positive than average NAO winter values (Beniston et al., 1997). This contrasted with the previous decades, which were very snowy (López-Moreno et al., 2020).

During the snow melting phase temperature is the key variable and trends show a robust century rise. In fact, the climate warming of ca. 1ºC observed in the Iberian mountains since the end of the Little Ice Age (Oliva et al., 2018) is one of the factors that determined the decrease of SD and snow cover duration at the Pyrenees from 1958 to 2017 (López-Moreno et al., 2020b). Even though the rising temperature at high elevations (>2000 m) practically did not impact HN during the coldest months of the snow season (Figure 6). At the whole mountain range, the temperature increased (ca. 0.3ºC/decade) in autumn and spring since 1950 (OPCC, 2019), which might determine a shortening of the seasonal cumulative HN. Results exposed, however, a (non-statistically significant) slight increase of the seasonal cumulative HN since 1985 or 2000 years to 2020 in the eastern Catalan Pyrenees. Moreover, the negative trends of the N western sector could be linked with low-frequency climate modes oscillation. For the future, climate projections point out an increase of precipitation over the eastern Catalan Pyrenees by the end of the 21st century, in contrast to the western part of the range where precipitation is expected to decrease (Amblar-Francés et al., 2020). Therefore, the seasonal cumulative HN trends at high altitudes of the study area may remain constant in the future, if temperature is cold enough to allow solid precipitation.

Winter snow in Europe has decreased less in the high elevations than in the lowlands, and even in some cases increased (Räisänen, 2008). Indeed, for the future, a slight increment of winter precipitation at high altitudes is expected, even though the decrease of snow in early autumn and late spring may shorten the snow season (Räisänen, 2008). Observational data from the Alps reveal similar patterns. In the last century, snow accumulation at the Swiss Alps showed also large decadal variability, with minimum values found in the late 1980s and 1990s (Scherrer et al., 2013). In terms of SD, the southern parts of Austria and Switzerland showed a decrease from 1961 to 2012 (up to -12 cm/decade at ca. 2000 m) although in the NE of Austria no trend has been found (Scöner et al., 2019). In addition, trends in the number of days of snow on the ground are generally negative at all altitudes in the order of 3 days/decade (Scöner et al., 2019).

Recent climate trends also determine two important feedbacks affecting mountain ecosystems. The first one, and linked with snowfall, occurs principally during the late months of the snow season. Due to a warmer climate, rain on snow events are likely to increase in the Alpine areas enhancing floods (Beniston et al., 2016). The second one, and in terms of snow cover, can be applied to other regions where soil is covered by snow during certain time per year. The albedo of the snow free areas lets retain more solar radiation, which enhances the warming tendency. This effect is quantified at ca. 4ºC on near-surface temperature during spring at Swiss Alps (Scherrer et al., 2012). In Iberian mountain ranges, years with less snow condition colder ground temperatures than snow-rich years, when the snow isolates the ground from atmospheric oscillations; this has major implications for terrestrial ecosystems in high altitude regions (Oliva et al., 2014; Gómez-Ortiz et al., 2019).

4.2 Circulation weather types

Eight large scale flows determine the atmospheric circulation variability and the snow regime in the western and eastern Catalan Pyrenees, explaining a variance of 86% (Figure 7). The southern displacement of the circumpolar front from October to April brings advective winter storms and snow in the Pyrenees summits. In contrast, subtropical high-pressure systems lead stable air masses, usually warm, which can reduce the snow records considerably.

The low pressures systems over the Atlantic bring high amounts of HN (Figure 9). They are represented by CT 1, 4 and 5, being in the first case more frequent in autumn (19%), in the second one in spring (18%) and in the latest during winter (14%; Table 4). CT 1 closely resembles CT 5 and could be clustered in one group. In both situations a high-pressure system is established near Azores and a low pressure system in Arctic latitudes allow cold air flow towards subtropical latitudes (Figure 8). CT 1 is defined by a W air flow that affects mostly at the western sector of the Catalan Pyrenees decreasing towards the eastern, whilst CT 5 generates a NW advection bringing snow on the N face of the western Catalan Pyrenees and also at Malniu station (Figure 9 and 10). The third Atlantic low area is the CT 4. At synoptic scale a high-pressure system is settled at the S of Azores, with a maritime polar air mass located in the NW of Iberia that affects practically the whole peninsula. A SW advection of moist and temperate air masses brings heavy precipitation and snow on the elevated zones. Practically half of the total of the HN in a season is recorded during CT 4 episodes at the southern slopes of the Catalan Pyrenees (Figure 8 and 9). On the contrary, during NW air flows the N mountain massifs receive the major precipitation quantities (Esteban et al., 2009) leading to heavy snowfalls at Andorra (Esteban et al., 2005). The majority of the snow days at the southern

slopes of the Pyrenees were recorded under NW CT, both at low (ca. 1000 m; Buisan et al., 2014) or at high altitude areas (>1800 m; Navarro-Serrano et al., 2017).

No significant trends of reduction of Atlantic low pressure systems related to precipitation were found, which seem to explain the non-statistically trends of HN. Nonetheless, the reduction of Atlantic advections since 1958 to 2017 explains the statistically significant reduction of snow days and snow cover at >2100 m, together with the long term trend of climate warming (López-Moreno et al., 2020b).

Mediterranean low-pressure systems are a second cluster of snow events, and can be classified into the CT 2 and 7. CT 2 is defined by an anticyclonic system over the British Isles and a weak eastern Mediterranean flow generated partially by an orographic pressure dipole on the Pyrenees (Bénech et al. 1998; Gonzalez et al. 2018). These low pressures at the E can generate snow in the high elevation sectors concentrated during spring (19%), especially at the eastern fridge and losing intensity towards the W of the range (Figure 10). CT 7 is a synoptic configuration with a low pressure area displaced towards the Mediterranean and a weakened high-pressure system established in the western Iberia sector. N and NE air flows generate wet conditions triggering snow episodes concentrated at Malniu, Núria and especially at the N face of the western Catalan Pyrenees. In fact, at Sasseuva and Bonaigua the maximum HN was recorded during CT 7 episodes, instead of CT 4, which is the general pattern. The CT 7 shows a clear N-S snow accumulation differences along the mountain range. The same pattern was observed with rainfall (Esteban et al., 2009; Lemus-Canovas et al., 2018).

A third cluster of CT is associated with anticyclonic conditions. They are the CT 3, 6 and 8 and are characterized by below mean HN at almost all the stations studied (Figure 9). In case of CT 3, an Atlantic anticyclone extension over Iberia produces few snow episodes and negative snow balance. The CT 6, is driven by a high-pressure system over central Europe that generates a wind flow of continental air masses, dry and cold. Stable weather conditions prevail, and in case of solid precipitation the spatial pattern is similar to CT 2. Finally, the CT 8 guarantees numerous sun hours over most Pyrenean massifs. It is a typical CT during winter months (20% of the days), especially in January when it usually persists for several days and rarely brings snow.

4.3 Low frequency climate modes

Our results showed weak correlations between seasonal cumulative HN and AO/NAO patterns, and significant correlations were only found in particular stations. In November and December, an association with the NAO was found at Boí (r = -0.50, p-value<=0.01), Port del Comte (r = -0.50, p-value<=0.01) and Cadí-Nord stations (r = -0.48, p-value<=0.01; not figure shown). Along the winter season no significant correlation is found with AO/NAO index, except with the first pattern at Boí station (r = -0.37, p-value<=0.001). Whereas in eastern Iberia a weak connection between winter precipitation and NAO was detected (e.g., Martín-Vide et al., 2006), in the western and central Pyrenees a high correlation between snowfall and NAO was found (r = -0.6; López-Moreno et al., 2005; 2011). This is explained by the W to E orientation of the mountain range protects the eastern sector from the W wind. However, these correlations in the Pyrenees are complex and uneven, as shown by the lack of correlation between NAO and snowpack at northern slopes of the mountain range (Alonso-González et al., 2020). High correlations of the NAO with precipitation during winter were found in other Iberia mountain systems, such as the Cantabrian Mountains (r = -0.60; López-Moreno et al., 2011) or Sierra Nevada (r = -0.70) that presents also the same shadow effects of the precipitation over the eastern stations (Oliva et al., 2008).

The EA is a similar teleconnection pattern to the NAO. The difference lies in the centers of action, placed in a southern position in case of the EA. The EA teleconnection pattern is negatively correlated with HN in most stations during autumn and winter (Figure 11). The higher and significant correlations are found at Ulldeter station during autumn (r = -0.25, p-value<=0.001) and at Malniu along winter (r = -0.37, p-value<=0.001). The association found is explained because of the higher exposure of these stations to CT associated to Mediterranean flows over the Pyrenees (Figure 9, CT 2 and 7), which are related with EA negative phases (e.g., Vicente-Serrano et al., 2006). Results exposed are consistent with previous ones which identified a negative correlation between precipitation in southern Europe and the EA index throughout autumn and winter, together with a correlation between the negative EA phases and low winter temperatures (Comas-Bru et al., 2018).

Some correlations were also observed between HN and the EAWR. The EAWR positive values are related with positive anomalies over the Euroasian continent and low pressures over the N Caspian Sea and mid latitude areas of the Atlantic sea (Barnston et al., 1987). Results showed that negative phases of the EAWR are slightly correlated with the seasonal cumulative HN recorded in the eastern Catalan Pyrenees in autumn and winter, with a maximum correlation observed in Espot station during winter (r = -0.31, p-value<=0.05). Negative phases of the

EAWR during winter are related with wet conditions over the Mediterranean region (Barnston et al., 1987). These situations are linked with local depressions producing precipitation from October to March (Rodrigo et al., 2008). Whereas CT associated with E flow over the Pyrenees are linked with positive phases of the EAWR, a negative correlation has been found with CT associated with W flows (Vicente-Serrano et al., 2006). This explains that the highly correlated stations in spring, majorly the eastern Catalan Pyrenees stations ($r \sim 0.40$), accumulate more snow in E advections than with W and NW ones. In addition, it should be noted that snow stations correlated with the EAWR in spring are in the same grade correlated with the SOI lagged values. Generally, the snowy years recorded in these stations correspond to higher than normal lagged SOI values. For instance, the lowest spring HN years (i.e., 2005, 2007 or 2014 spring seasons) were related with negative values of the previous autumn SOI (-4.9, -7.2, -8.1; respectively). On the other side, snowy spring seasons (i.e., 2009, 2010 or 2018) were linked with high autumn SOI values (14.3, 20, 8.9; respectively). These results confirm former studies based on rainfall at eastern Iberia (Rodó et al., 1997). Notwithstanding results exposed are statistically not significant and future studies might corroborate these earlier correlations found.

Positive phases of the SCAND present a high pressure system over Scandinavian, allowing SW, W and NW advections (e.g., Vicente-Serrano et al., 2006). The seasonal cumulative HN correlation with the SCAND teleconnection pattern is high throughout winter ($r \sim 0.30$). In fact, in the core months of the season, positive phases have the same capacity to explain low to medium HN variability ($r \sim 0.3$) in the western and easternmost area of the Catalan Pyrenees. The highest correlation is measured at Boí ($r = 0.36$, p-value<=0.001), Ulldeter ($r = 0.31$, p-value<=0.01) and Port del Comte ($r = 0.31$, p-value<=0.01). Practically the same correlation ($r = 0.2$) was measured during winter in snow poles located >2200 m of the western and central Pyrenees (Revuelto et al., 2012). A negative correlation has been found during autumn, but any capacity to explain HN variability in spring.

Finally, the WeMO positive phases are related with CT associated with W, NW and N advections, while on the contrary, negative values are linked with E advections (Martín-Vide et al., 2006). At Sasseuva, Bonaigua and Certascan (in the N aspect of the western Catalan Pyrenees) this singular teleconnection pattern has the highest ($r > 0.5$) and the most significant capacity to explain HN variation (Figure 11). No seasonal dependence is observed, although the stronger correlations are observed in spring. In this sector, WeMO is also correlated with rainfall at lower elevations (Lopez-Bustins et al., 2019). In the eastern Catalan Pyrenees, the correlation between WeMO and HN is low and decreased during the snow season. The long-

scale WeMO trend has been marked by positive values in the last century (1900-2000; Oliva et al., 2006). Nevertheless, negative phases prevailed at the beginning of the 21st century, which has been attributed to the increase of sea temperatures (Lopez-Bustins et al., 2020). Therefore, the negative HN trend observed at Sasseuva, Bonaigua and Certascan stations (Figure 5 and 6) can be explained by the large scale climate variability of WeMO values.

In short, there is no unique teleconnection pattern which determines the snow regime over the eastern Catalan Pyrenees. The complex relief configuration of the Pyrenees condition that several synoptic patterns control the timing and amount of snow precipitation due to: (i) the orography of the mountain ranges of the surroundings play a relevant role generating rain shadow effects; (ii) the range of different directional CT that affect the study area, which usually represent contrary phases of low frequency atmospheric modes; and (iii) the exposure to different wind flows of a massif where a snow station is placed determine the grade of correlation with each low-frequency mode of circulation.

5. Conclusions

Climate warming will reduce the extent of the cryosphere in the future decades (IPCC, 2019). Therefore, a better understanding of the spatio-temporal patterns of snow is crucial for assessing the impact of the coming climate scenarios. With this aim, we examined the snow records at high elevations of the Catalan Pyrenees, a sector where studies conducted with direct observations were not conducted to the date.

Two distinct snow patterns were identified between the different sectors of the eastern fringe of the Pyrenees. The western Catalan Pyrenees recorded the highest seasonal cumulative HN values (>430 cm per season), practically the double of the eastern sector. In this sense, the mountain range acts as a relief barrier depending on the prevailing synoptic pattern. Under Mediterranean cyclogenesis episodes, the orographic uplifting generates abundant snow, spatially concentrated on the N face of the western Catalan Pyrenees and at Malniu and Núria stations. HN diminishes downward of the moist advection: E (W) advections affect mainly to the eastern (western) side of the area of study as weakens to the west (east). The Atlantic low pressure systems were identified as the major driver of snow accumulation. Indeed, the cold and wet fronts (CT 1 and 5) provide snow, majorly at the N face of the western Catalan Pyrenees. In the majority of the stations, almost half of the HN for a season was recorded with a singular CT: an Atlantic low pressure placed just at the NW of the Iberian Peninsula. Under this synoptic

situation, SW wet and mild air flow leads to abundant snow on the high elevation areas analyzed. The effect of each CT over the Pyrenees sectors determined the snow timing (e.g., winter is the snowiest period in the N western Catalan Pyrenees) and also the observed snow trends.

The orography and the exposure to different wind flows influence the correlation of each low frequency climate mode. Along the core months of the season, the negative phases of the EA and AO and positive of the SCAND were correlated with HN ($r \sim 0.3$). In spring, positive phases of EAWR were correlated with HN mostly in the eastern area of the western Catalan Pyrenees and at the eastern Catalan Pyrenees ($r \sim 0.4$). At the N western Catalan Pyrenees, the HN variation is attributed to the WeMO pattern ($r = 0.50$, p-value<=0.05). Therefore, the negative seasonal cumulative HN trend observed in this region can be attributed to the negative oscillation of the WeMO of the last two decades.

From 1985 and the earliest 2000 to 2020, an upward seasonal cumulative HN trend was recorded within the eastern Catalan Pyrenees (Kendall's τ value around 0.1, non-statistically significant). On the opposite side, negative seasonal cumulative HN trends (Kendall's τ value around 0.1, non-statistically significant) were found at the N western Catalan Pyrenees. Climate models project an increase of temperature (>1ºC) but also precipitation (>10%) toward the end of the 21st century at the eastern Catalan Pyrenees, and a reduction of precipitation on the western sector. Future studies should assess if the seasonal cumulative HN trends observed at the highest land will remain constant.

This study remarks the relevance of meteorological measurements at high elevation zones. Snow observations at mountain environments are usually scarce and time limited. However, they provide valuable information for snow-related activities as well as for the local climate and ecosystem dynamics. The high inter-seasonal variability of snow, together with snow cover extent variations and the rate of snow melting are potential drivers of modifications on soil thermal regime, altering the number and timing of freeze-thaw cycles or changing the vegetation phenology. Therefore, future research in the study area should focus on the interactions between the cryosphere and geoecological dynamics.

Acknowledgments

This work frames within the research topics examined by the research groups "Antarctic, Artic,

Alpine Environments-ANTALP" (2017-SGR-1102), "Climatology Group" (2017-SGR-1362) and "Paisatge i paleoambients a la muntanya mediterrània" (2014-SGR-0373) of the University of Barcelona. Marc Oliva is grateful for the support of the Ramón y Cajal research program (RYC-2015-17597). We thank the SMC and ICGC of the 'Department of Territori i Sostenibilitat' of the Catalan Government (Generalitat de Catalunya) for the data provided.

6. References

Alonso-González, E., López-Moreno, J.I., Navarro-Serrano, F.M and Revuelto, J. (2020) Impact of North Atlantic Oscillation on the Snowpack in Iberian Peninsula Mountains. *Water*, 12, 105. https://doi.org/10.3390/w12010105.

Amblar-Francés, P., Ramos-Calzado, P., Sanchis-Lladó, J., Hernanz-Lázaro, A., Peral, C., Navascués, B., Dominguez-Alonso, M., Pastor, M. and Rodriguez-Camino, E. (2020) High resolution climate change projections for the Pyrenees region. *Advances in Science and Research*, 17, 191-208. https://doi.org/10.5194/asr-17-191-2020**.**

Barnston, A.G. and Livezey, R.E. (1987) Classification, Seasonality, and Persistence of Low Freqüency Atmospheric Circulation Patterns. *Monthly Weather Review*, 115, 1083-1126. https://doi.org/10.1175/1520-0493(1987)115<1083:CSAPOL>2.0.CO;2.

Bénech, B., Koffi, E., Druilhet, A., Durand, P., Bessemoulin, P., Campins, J., Jansa, A. and Terliuc, B. (1998) Dynamic Characteristics of Regional Flows around the Pyrénées in View of the PYREX Experiment. Part I: Analysis of the Pressure and Wind Fields and Experimental Assessment of the Applicability of the Linear Theory. Journal of Applied Meteorology. 37. 32-52. https://doi.org /10.1175/1520-0450(1998)037<0032:DCORFA>2.0.CO;2

Beniston, M., Diaz, H. F., and Bradley, R. S. (1997) Climatic Change at High Elevation Sites; A Review. *Climate Change*. 36, 233-251.

Brown, R., and Robinson, D. (2011) Northern Hemisphere spring snow cover variability and change over 1922–2010 including an assessment of uncertainty. *The Cryosphere*, 5(1), 219-229, https://doi:10.5194/tc-5-219-2011.

591 Buchmann, M , Begert, M., Brönnimann, S and Marty, C. (2020) Evaluating the robustness of
592 snow climate indicators using a unique set of parallel snow measurement series. *International*
593 *Journal of Climatol*ogy, 1-11. https://doi.org/10.1002/joc.6863
594
595 Buisán, S. T., Sanz, M. A. and López-Moreno, J. I. (2014) Spatial and temporal variability of
596 winter snow and precipitation days in the western and central Spanish Pyrenees. *International*
597 *Journal of Climatology*, 35, 259-274. https://doi.org/10.1002/joc.3978.
598
599 Buisán, S. T., López-Moreno, J. I., Sanz, M. A., and Korchendorfer,J. (2016) Impact of weather
600 type variability on winter precipitation, temperature and annual snowpack in the Spanish
601 Pyrenees. *Climate Research*, 69, 79-92. https://doi.org/10.3354/cr01391
602
603 Comas-Bru, L., and Hernández, A. (2018) Reconciling North Atlantic climate modes: revised
604 monthly indices for the East Atlantic and the Scandinavian patterns beyond the 20th century,
605 *Earth System Science Data,* 10(4), 2329-2344. https://doi.org/10.5194/essd-10-2329-2018.
606
607 Climate Prediction Center (CPC). (2019) Northern Teleconnection Patterns.
608 https://www.cpc.ncep.noaa.gov/data/teledoc/telecontents.shtml.
609
610 Esteban, P., Jones, P. D., Martín-Vide, J., and Mases, M. (2005) Atmospheric circulation
611 patterns related to heavy snowfall days in Andorra, Pyrenees. *International Journal of*
612 *Climatology,* 25(3), 319-329. https://doi.org/10.1002/joc.1103.
613
614 Esteban, P., Ninyerola, M., and Prohom, M. (2009) Spatial modelling of air temperature and
615 precipitation for Andorra (Pyrenees) from daily circulation patterns. Theor. Appl. Climatol. 96:
616 43-56. https://doi.org/10.1007/s00704-008-0035-3.
617
618 El Kenawy, A., López-Moreno, J.I., and Vicente-Serrano, S.M. (2012) Trend and variability of
619 temperature in northeastern Spain (1920-2006): linkage to atmospheric circulation. *Atmospheric*
620 *Research*, 106, 159-180. http://dx.doi.org/10.1016/j.atmosres.
621 García-Ruiz, J.M., López-Moreno, J.I., Vicente-Serrano, S., Lasanta, T., and Beguería, S.
622 (2011) Mediterranean Water Resources in a Global Change Scenario. *Earth-Science Reviews*,
623 105, 121-139. http://dx.doi.org/10.1016/j.earscirev.2011.01.006.
624

Gómez-Ortiz, A., Oliva, M., Salvador-Franch, F., Palacios, D., Tanarro, L.M., Sanjosé-Blasco, J.J. and Salvà-Catarineu, M. (2019) Monitoring permafrost and periglacial processes in Sierra Nevada (Spain) from 2001 to 2016. *Permafrost and Periglacial Processes*, 30 (4), 278-291.

Gonzalez, S., Callado, A., Werner, E., Escribà, P. and Bech, J. (2018) Coastally trapped disturbances caused by the tramontane wind on the northwestern Mediterranean: Numerical study and sensitivity to short-wave radiation. *Quarterly Journal of the Royal Meteorological Society* 144, 1321-1336. https://doi.org/10.1002/qj.3320.

Houze, R. (2012) Orographic effects on precipitating clouds. *Reviews of Geophysics*, 50, 1001. https://doi.org/10.1029/2011RG000365.

IPCC: Technical Summary (2019) in: IPCC Special Report on the Ocean and Cryosphere in a Changing Climate, edited by: Pörtner, H.- O., Roberts, D. C., Masson-Delmotte, V., Zhai, P., Poloczanska, E., Mintenbeck, K., Tignor, M., Alegría, A., Nicolai, M., Okem, A., Petzold, J., Rama, B., and Weyer, N. M., available at: https://www.ipcc.ch/site/assets/uploads/sites/3/2019/11/ 04_SROCC_TS_FINAL.pdf (last access: 16 October 2020).

Kalnay, E., M., Kanamitsu, R., Kistler, W., Collins, D., Deaven, L., Gandin, M., Iredell, S., Saha, G., White, J., Woollen, Y., Zhu, M., Chelliah, W., Ebisuzaki, W., Higgins, J., Janowiak, K.C., Mo, C., Ropelewski, J., Wang, A., Leetmaa, R., Reynolds, R., Jenne, R., and Jospeh, D. (1996) The NCEP/NCAR 40-Year Reanalysis Project. *Bulletin American Meteorological Society*, 77, 437-472. http://dx.doi.org/10.1175/1520-0477(1996)077<0437:TNYRP>2.0.CO;2

Kendall, M.G. (1948) Rank Correlation Methods. Oxford: Griffin.

Maris, M., Giraud, G., Durand, Y., Navarre, JP., and Mérindol, L. (2009) Results of 50 years of climate reanalysis in the French Pyrenees (1958-2008) using the SAFRAN and CROCUS models. In Proceedings of ISSW2009. International Snow Science Workshop 2009, Davos, Switzerland.

Martín-Vide, J., Brunet, M., Prohom, M., and Rius, A. (2011) Els climes de Catalunya. Present i tendències recents. In: Llebot, J.E. (Ed.), Segon informe sobre el canvi climàtic a Catalunya. Institut d'Estudis Catalans i Generalitat de Catalunya. 39-72.

Martín-Vide, J., and Lopez-Bustins, J.A. (2006) The Western Mediterranean Oscillation and rainfall in the Iberian Peninsula". *International Journal of Climatology*, 26 (11), 1455-1475. https://doi.org/10.1002/joc.1388.

Notarnicola, C. (2020) Hotspots of snow cover changes in global mountain regions over 2000–2018. Remote Sens. Environ. 243 (111), 781. https://doi:10.1016/j.rse.2020. 111781.

OPCC-CTP (2018). Climate change in the Pyrenees: Impacts, vulnerabilities and adaptation Bases of knowledge for the future climate change adaptation strategy in the Pyrenees. 147 pp, Jaca, Spain. https://www.opccctp.org/sites/default/files/editor/opcc-informe-en-paginas.pdf. (last access: 16 October 2020).

Oliva, M., Gómez-Ortiz, A., Salvador-Franch, F., Salvà-Catarineu, M., Pereira, P. and Geraldes, M. (2014) Long term soil temperature dynamics in the Sierra Nevada, Spain. *Geoderma*, 235-236: 170-181.

Oliva, M. and Moreno, I. (2008) Sierra Nevada, nexo entre dos patrones de teleconexión: La NAO y la WeMO. Sigró, J.; Brunet, M. & Aguilar, E. (eds.): Cambio Climático Regional y sus Impactos, Publicaciones de la Asociación Española de Climatología, Serie A (6):199-208. In IX Congreso de la AEC, Almería, 729-738.

Oliva, M., Lopez-Bustins, J., Barriendos, M., Muedra, C. and Martín-Vide, J. (2006) Reconstrucción histórica de la Oscilación del Mediterráneo Occidental (WeMO) e inundaciones en el levante peninsular (1500-2000). In: Actas V Congreso de La Asociación Española de Climatología (AEC). Zaragoza, 241–250.

Oliva, M., Serrano, E., Gomez-Ortiz, A.G., Gonzalez-Amuchastegui, M.J., Nieuwendam, A., Palacios, D., Perez-Alberti, A.P., Pellitero, R., Ruiz, J., Valcarcel, M., Vieira, G. and Antoniades, D. (2016) The periglaciation of the Iberian Peninsula. Spatial and temporal variability. *Quaternary Science Reviews*, 137, 176-199. https://doi.org/10.1016/j.quascirev.2016.02.017.

693 Lemus-Canovas, M., Lopez-Bustins, J.A., Martín-Vide J. and Royé, D. (2019) "synoptReg: An
694 R package for computing a synoptic climate classification and a spatial regionalization of
695 environmental data. *Environmental Modelling & Software*, 118, 114–119.

696 Lemus-Canovas, M., Ninyerola, M., Lopez-Bustins, J.A., Manguan, S., and García-Sellés, C.
697 (2018) A mixed application of an objective synoptic classification and spatial regression models
698 for deriving winter precipitation regimes in the Eastern Pyrenees. *International Journal of*
699 *Climatology*, https://doi.org/10.1002/joc.5948.
700
701 Lopez-Bustins, J.A. and Lemus-Canovas, M. (2019) The influence of the Western
702 Mediterranean Oscillation upon the spatio-temporal variability of precipitation over Catalonia
703 (northeastern of the Iberian Peninsula). *Atmospheric Research*, 236, 104-819.
704 https://doi.org/10.1016/j.atmosres.2019.104819.
705
706 Lopez-Bustins, J.A., Arbiol-Roca, L., Martín-Vide, J., Barrera-Escoda, A. and Prohom, M.
707 (2020) Intra-annual variability of the Western Mediterranean Oscillation (WeMO) and
708 occurrence of extreme torrential precipitation in Catalonia (NE Iberia). *Natural hazards and*
709 *earth system sciences*, 20. 2483-2501. https://doi.org/10.5194/nhess-20-2483-2020.

710 Lopez-Bustins, J., Martín-Vide, J. and Sanchez-Lorenzo, A.(2008) Iberia winter rainfall trends
711 based upon changes in teleconnection and circulation patterns. *Global and Planetary Change*,
712 63, 171. https://doi.org/10.1016/j.gloplacha.2007.09.002

713 López-Moreno, J. I. (2005) Recent variations of snowpack depth in the central Spanish
714 Pyrenees. *Arctic Antarctic Alpine Research*, 37(2). https:/doi.org/10.1657/1523-0430(2005)037.
715
716 López-Moreno, J. I., Gascoin, S., Herrero, J., Sproles, E. A., Pons, M., Alonso-González, E.,
717 Hanich, L., Boudhar, A., Musselman, K. N., Molotch, N. P., Sickman, J., and Pomeroy, J.
718 (2017) Different sensitivities of snowpacks to warming in Mediterranean climate mountain
719 areas. *Environmental. Research Letters*, 12(7). https://doi.org/10.1088/1748-9326/aa70cb, 2017.
720
721 López-Moreno, J.I., Pomeroy, J.W., Alonso-González, E., Morán-Tejeda, E. and Revuelto, J.
722 (2020a) Decoupling of warming mountain snowpacks from hydrological regimes.
723 *Environmental Research Letters*, 11-15. https://doi.org/10.1088/1748-9326/abb55f

724 López-Moreno, J.I., Soubeyroux, J.M., Gascoin, S., Alonso-González, E., Durán-Gómez, N.,
725 Lafaysse, M., Vernay, M., Carmagnola, C. and Morin, S. (2020b) Long-term trends (1958–

2017) in snow cover duration and depth in the Pyrenees. *International Journal of Climatology*, 1-15. https://doi.org/10.1002/joc.6571

López-Moreno, J.I. and Vicente-Serrano, S.M. (2007). Atmospheric circulation influence on the interannual variability of snowpack in the Spanish Pyrenees during the second half of the 20th century. *Hydrology Research* (2007) 38 (1): 33-44. https:/doi.org/10.2166/nh.2007.030

López-Moreno, J.I., Vicente-Serrano, S.M., Morán-Tejeda, E., Lorenzo-Lacruz, J., Zabalza, J., Kenawy, A. and Beniston, M. (2011) Influence of Winter North Atlantic Oscillation Index (NAO) on Climate and Snow Accumulation in the Mediterranean Mountains.

López-Palomeque, F. (1996) Turismo de invierno y estaciones de esquí en el Pirineo catalán. *Investigaciones Geográficas*, 15, 19-39.

Marty, C. and Meister, R. (2012) Long-term snow and weather observations at Weissfluhjoch and its relation to other high-altitude observatories in the Alps. *Theoretical and Applied Climatology*, 110(4), 573–583.

Morán-Tejeda, E., López-Moreno, J. I. and Beniston, M. (2013) The changing roles of temperature and precipitation on snowpack variability in Switzerland as a function of altitude, Geophyical Research Letters., 40, 2131-2136, https://doi.org/10.1002/grl.50463

Navarro-Serrano, F. and López-Moreno, J.I. (2017) Spatio-Temporal analysis of snowfall events in the Spanish Pyrenees and their relationship to Atmospheric Circulation. *Cuadernos de Investigación Geográfica.* 43(1), 233-254.

Salvador Franch, F., Salvà, G., Vilar, F and García, C. (2014) Nivometría y perfiles de innivación en Núria (1.970 m, Pirineo Oriental): 1985-2013. In IX Congreso de la AEC, Almería, 729-738.

Salvador-Franch, F., Salvà, G., Vilar, F. and García, C. (2016) Contribución al análisis nivométrico del Pirineo Oriental: La Molina, período 1956-1996. In X Congreso Internacional AEC: Clima, sociedad, riesgos y ordenación del territorio, Alicante, 365-375.

Scherrer, S.C., Ceppi, P., Croci-Maspoli, M. and Appenzeller C. (2012) Snow-albedo feedback and Swiss spring temperature trends. *Theoretical and Applied Climatology*. 110(4), 509-516. https://doi.org/10.1007/s00704-012-0712-0.

Scherrer, S.C., Wüthrich, C., Croci-Maspoli, M., Weingartner, R. and Appenzeller, C. (2013) Snow variability in the Swiss Alps 1864–2009. *International Journal of Climatology*, 33(15), 3162–3173. https://doi.org/10.1002/joc.3653.

Schöner, W., Koch, R., Matulla, C., Marty, C. and Tilg, A.M. (2019) Spatiotemporal patterns of snow depth within the Swiss Austrian Alps for the past half century (1961 to 2012) and linkages to climate change. *International Journal of Climatology*. 39 (3), 1589-1603. https://doi.org/10.1002/joc.5902.

Servei Meteorològic de Catalunya (SMC). (2008) Atlas climàtic de Catalunya (ACDC). https://www.meteo.cat/climatologia/atles_climatic/ (last access: 30 October 2020).

Servei Meteorològic de Catalunya (SMC). (2011) Les estacions meteorològiques automàtiques (EMA).https://static-m.meteo.cat/wordpressweb/wp content/uploads/2014/11/18120559/Les_Estacions_XEMA.pdf. (last access: 30 October 2020).

Pepin, N.and Kidd, D. (2006) Spatial temperature variation in the Eastern Pyrenees. *Weather*. 61(11), 300-310.

Peña-Angulo, D., Vicente-Serrano, S., Domínguez-Castro, F., Murphy, C., Reig, F., Tramblay, Y., Trigo, R., Luna, M. Y., Turco, M., Noguera, I., Aznárez-Balta, M., Garcia-Herrera, R., Tomas-Burguera, M., and Kenawy, A. (2020) Long-term precipitation in Southwestern Europe reveals no clear trend attributable to anthropogenic forcing. *Environmental Research Letters*. https://doi.org/10.1088/1748-9326/ab9c4f.

Pineda, N., Esteban, P., Trapero, L., Soler, X. and Beck, C. (2010) Circulation types related to lightning activity over Catalonia and the Principality of Andorra. Phys. Chem. Earth 35, 469–476. https://doi.org/10.1016/j.pce.2009.12.009

Räisänen, J. (2008) Warmer climate: less or more snow?. *Climate Dynamics*. 30, 307–319. https://doi.org/10.1007/s00382-007-0289-y

Ramos, AM., Cortesi, N. and Trigo, RM. (2014) Circulation weather types and spatial variability of daily precipitation in the Iberian Peninsula. *Frontier in Atmospheric Science. 2, 25*. https://doi.org/10.3389/feart.2014.00025.

Revuelto, J., López-Moreno, J., Moran-Tejeda, E., Fassnacht, S., and Vicente-Serrano, S.M. (2012) Variabilidad interanual del manto de nieve en el Pirineo: tendencias observadas y su relación con índices de teleconexión durante el periodo 1985-2011. 1, in: Rodríguez, C., Ceballos, A., González, N., Morán, E., Pacheco, S., Hernández A. (Eds.). Asociación Española de Climatología, Madrid, pp. 613- 621.

Rodó, X., Baert, E., and Comín FA. (1997) Variations in seasonal rainfall in Southern Europe during the present century: Relationships with the North Atlantic Oscillation and the El Niño-Southern Oscillation. *Climate Dynamics*. 13, 275-284. https://doi.org/10.1007/s003820050165

Rodrigo, F. S. and Barriendos, M. (2008) Reconstruction of seasonal and annual rainfall variability in the Iberian Peninsula (16th– 20th Centuries) from documentary data. *Global Planet. Change*, 63, 243–257. https://doi.org/10.1016/j.gloplacha.2007.09.004

TICC (2017). El canvi climàtic a Catalunya: Resum executiu del Tercer informe sobre el canvi climàtic a Catalunya. Redacció: Xavier Duran, M. Josep Picó i Lluís Reales. Edició: Arnau Queralt. Barcelona: Generalitat de Catalunya: Institut d'Estudis Catalans, 2017.

Trigo, R., Xoplaki, E., Zorita, E., Luterbacher, J., Krichak, S., Alpert, P., Jacobeit, J., Sáenz, J., Fernández, J., González Rouco, J. F., García-Herrera, R., and Rodó, X. (2006) Chapter 3 Relations between variability in the Mediterranean region and mid-latitude variability. *Developments in Earth and Environmental Sciences*. 4. https://doi.org/10.1016/S1571-9197(06)80006-6.

Vicente-Serrano, S.M and López-Moreno, J.I. (2006) The influence of atmospheric circulation at different spatial scales on winter drought variability through a semiarid climatic gradient in north east Spain. *International Journal of Climatology*, 26, 1427-1456. https://doi.org/10.1002/joc.1387.

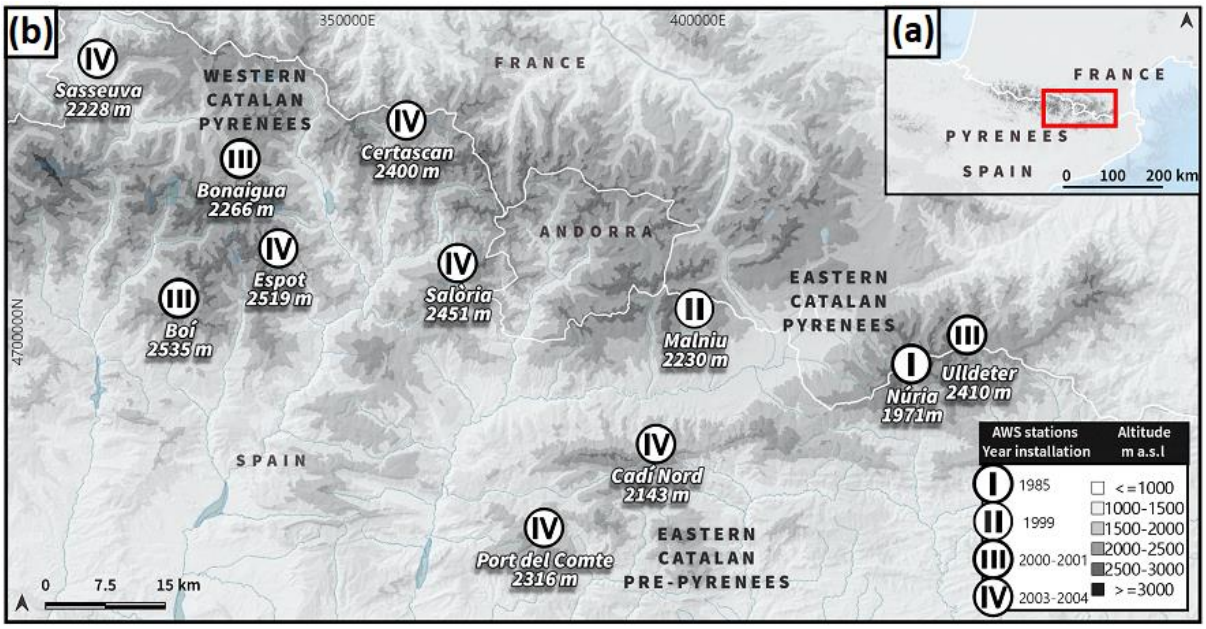

Figure 1 (a) Location map of the Pyrenees within the NE Iberian Peninsula, and (b) distribution of AWS across the Catalan Pyrenees and eastern Catalan Pre-Pyrenees. Data of the digital elevation model was downloaded from the European Environmental Agency (https://www.eea.europa.eu/data-and-maps/data/eu-dem).
.TIFF size: 233.36x121.18 mm (300 x 300 DPI)

Table 1. Main geographical characteristics of the AWS examined in this work, together with the time series length and missing data.

Geographical sectors	AWS	X/Y (UTM)	Altitude (m)	At.(1)	Med.(2)	A. H	Period analyzed	Years	Days analyzed (5)
Western Catalan Pyrenees	Sasseuva	42.77/0.73	2228	200	190	6	01-10-2004/ 31-03-2020	16	4281 (99.8)
	Bonaigua	42.61/0.98	2266	225	170	6	23-10-2001/31-03-2020	19	5076 (99.9)
	Boí	42.46/0.88	2535	230	185	6	09-10-2001/31-03-2020	19	5091 (99.8)
	Certascan	42.70/1.27	2400	245	145	6	01-10-2003/31-03-2020	17	4494 (98.9)
	Espot	42.53/1.05	2519	240	165	10	01-11-2003/31-03-2020	17	4540 (93.3)
	Salòria	42.51/1.36	2451	260	150	10	01-10-2004/31-03-2020	16	4281 (99)
Eastern Catalan Pre-Pyrenees	P Comte	42.18/1.52	2316	290	130	6	01-10-2004/31-03-2020	16	4281 (99.3)
	Cadí Nord	42.29/1.71	2143	300	110	6	01-10-2004 /31-03-2020	16	4281 (99.5)
Eastern Catalan Pyrenees	Malniu	42.46/1.78	2230	295	115	6	04-11-1999/31-03-2020	21	5558 (99.2)
	Núria	42.39/2.15	1971	330	80	10	01-01-1985//31-03-2020	36	12775(99)
	Ulldeter	42.42/ 2.24	2364 / 2410 (4)	350	75	6 /10 (4)	01-01-2000/31-03-2020	20	4938 (98.9)

Linear distance (km) to (1) Atlantic and (2) Mediterranean Sea. (3) Height of the anemometer (m). (4) Relocation of the AWS, at date 28-09-2011. (5) Number of days analyzed (% of the total days during the period analyzed).

Table 2. Descriptive statistics of the data measured at the different snow stations.

	Meteorological components		HN							SD (1)			
	Season		Day				Season			Day	Season		
AWS	TM (ºC)	Wind (m/s)	P25	P75	P90	Std. Dv. (cm)	Fr (days) (2)	Quantity (cm)	CV (3)	Max. (cm)	Quantity (cm)	Mean max. peak (cm)	Onset melting (3)
Sasseuva	1.03	1.60	2.3	10.9	17.8	7.8	51	403.0	28.1	226.1	63.0	136.6	24/03
Bonaigua	0.64	3.27	2.6	12.4	21.8	10.1	58	545.5	28.5	410.9	97.8	214.4	1/04
Boí	-0.30	4.13	2.3	12.3	24.2	11.5	49	470.2	31.4	347.9	69.2	152.8	11/04
Certascan	0.15	2.92	3.0	14.0	24.9	10.7	54	567.6	23.5	319.6	83.5	171.8	24/03
Espot	0.24	2.83	2.3	11.5	21.4	9.3	44	387.4	29.1	187.4	27.0	56.4	11/04
Salòria	0.08	4.61	1.8	7.1	14.0	7.1	39	230.8	45.2	137.0	11.9	26.8	24/03
P Comte	0.97	5.61	1.8	7.8	12.5	6.4	34	194.1	44.7	156.1	16.6	35.8	24/03
C.Nord	2.45	2.35	2.0	10.0	19.5	9.3	32	251.5	31.2	233.8	48.5	104.5	11/04
Malniu	2.24	1.84	2.2	10.6	18.9	9.6	38	313.3	24.0	126.2	17.8	48.0	5/03
Núria	3.59	2.42	2.0	11.4	20.4	4.1	34	283.1	31.4	170.0	14.9	40.2	7/02
Ulldeter	1.02	4.18	2.1	9.8	19.9	9.8	42	349.1	22.8	175.6	19.5	40.2	02/04

(1) Considering days with snow thickness >= 0.1 cm. (2) Coefficient of variation inter-seasonal. (3) Frequency (Fr.): HN days per season. (4) Day/Month seasonal avg. start of snow melting.

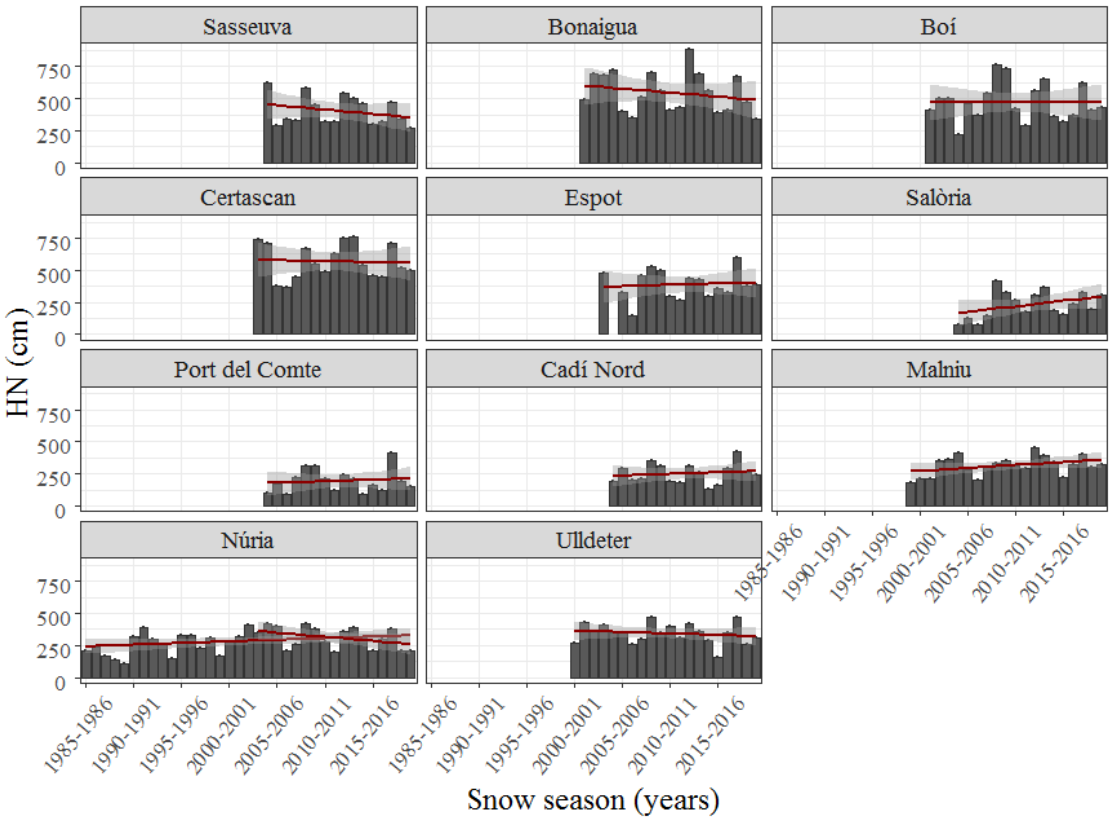

Figure 2. Evolution of the seasonal cumulative HN (cm) at each station. The red line indicates the linear regression and the grey zone indicates the confidence interval (at 95%).

.TIFF size: 230.18 x 169.33 mm (300 x 300 DPI)

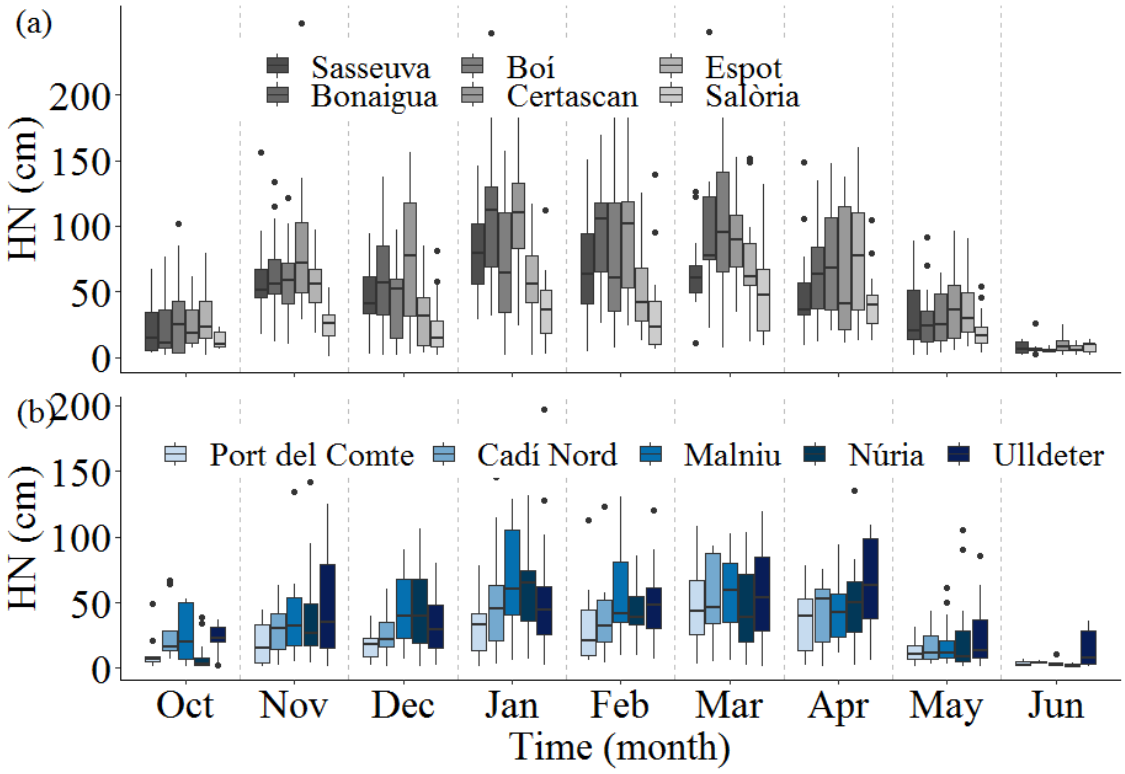

Figure 3. Monthly cumulative HN (cm). Stations are ordered according to the distance from the Atlantic to the Mediterranean Sea.

.TIFF size: 243.68 x 168.01 mm (300 x 300 DPI)

Table 3. Correlation and multiple linear regression between the snow parameters and geographical factors.

Snow Parameters	Pearson's correlation (r)				Multiple linear regression					
	Elev.	Lat.	Lon.	D. Seas	Intercept	Elev.	Lat.	Lon.	D. Seas	R^2
HN Season (Quantity)	0.34	0.74	-0.52	0.21	-2.04	1.68	4.80	-2.12	-4.99	0.61
HN season (CV)	-0.10	-0.45	-0.09	0.29	1.41	-9.16	-3.20	-7.00	2.33	0.45
HN season (Fr.)	0.33	0.83	-0.68	0.25	-1.30	1.03	3.14	-5.97	-1.88	0.78
HN day (>P75)	0.15	0.55	-0.30	0.07	-2.80	1.05	6.78	2.92	2.61	0.31
SD Season (Quantity)	0.02	0.60	-0.63	0.25	-2.30	-2.53	5.797	-3.19	-2.82	0.50
SD (Onset melt.)	0.53	0.07	-0.50	0.48	1.75	4.94	-4.11	-2.43	-2.50	0.49

Elev.: Elevation (m), Lat. and Lon.: Latitude and Longitude (º), respectively. D.Sea: Distance to the seas.

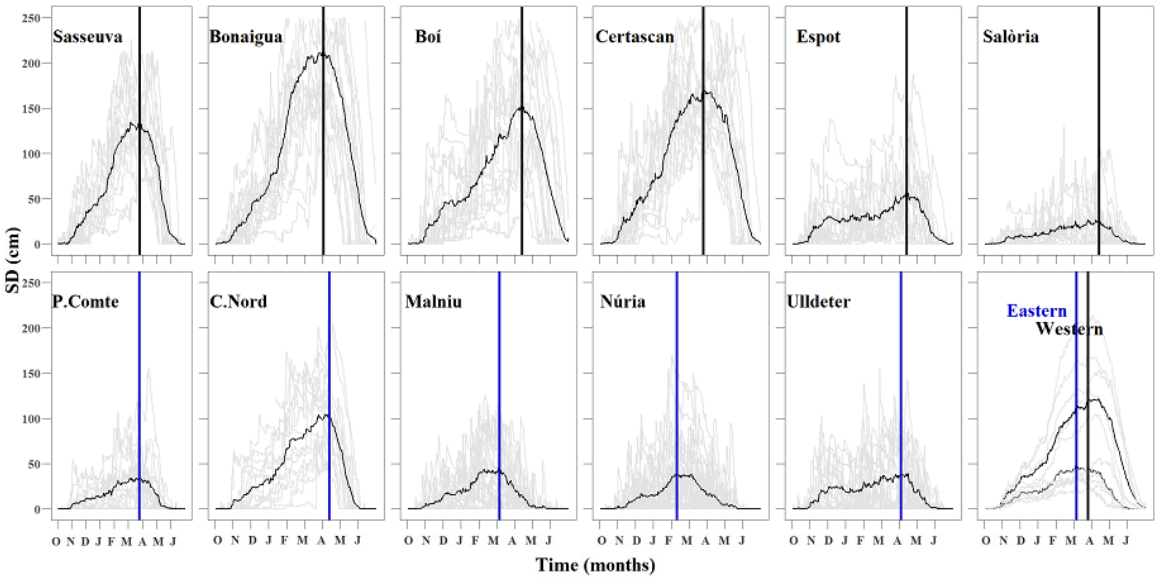

Figure 4. SD profiles of each station. The grey lines indicate the snow profile of each season whereas the black line the average SD for a season. The vertical line indicates the peak of snow accumulation, differentiating between the accumulation phase (left values respect the line) and the melting phase (right values).

.TIFF size: 241.30 x 121.44 mm (300 x 300 DPI)

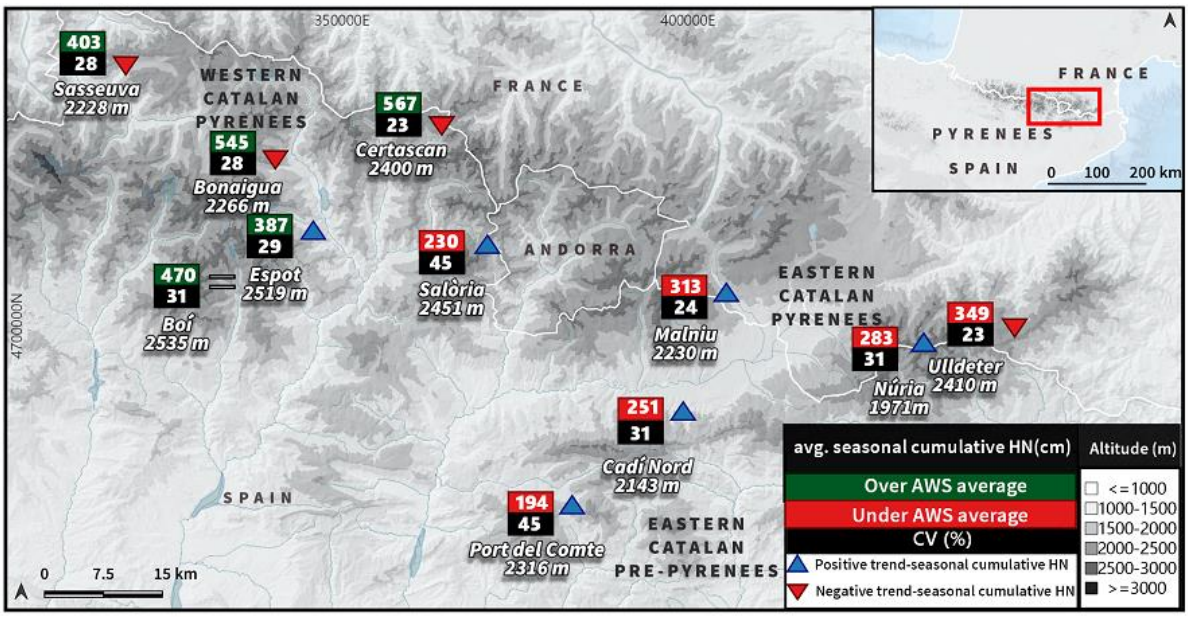

Figure 5. Spatial distribution of the seasonal cumulative HN, CV and seasonal cumulative HN trends recorded. All stations are not statistically significant, except Salòria seasonal trend, which is statistically significant at $p<0.05$. Data of the digital elevation model was downloaded from the European Environmental Agency (https://www.eea.europa.eu/data-and-maps/data/eu-dem).

.TIFF size: 233.89 x 120.91 mm (300 x 300 DPI)

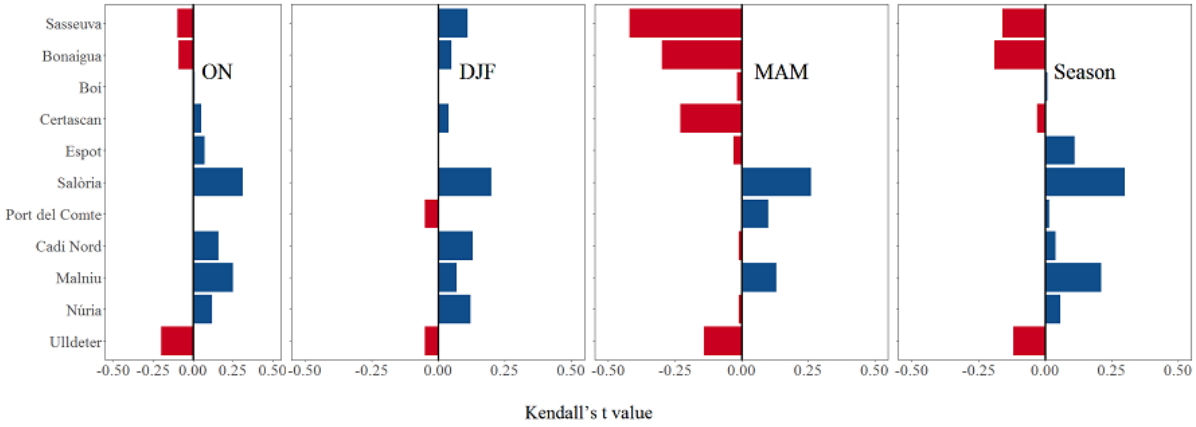

Figure 6. Mann-Kendall trend values of seasonal cumulative HN. All stations are not statistically significant, except Salòria season trend, which is statistically confidential at $p<0.05$.

.TIFF size: 238.68 x 93.07 mm (300 x 300 DPI)

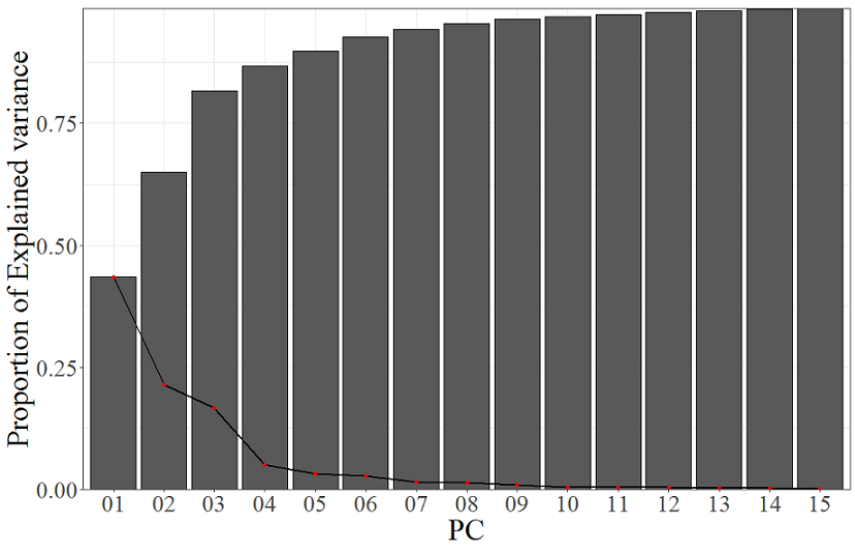

Figure 7. Scree test**.** Vertical axis shows the portion of explained variance and horizontal axis the present principal components.

.TIFF size: 219.07 x 140.229 mm (300 x 300 DPI)

Table 4. Relative frequency of each CT in all days of the last two decades.

	CT							
	1	2	3	4	5	6	7	8
ON	18.9	11.06	7.58	16.7	11.41	15.98	6.24	12.04
DJF	15.43	9.89	13.10	7.32	13.54	11.45	8.48	20.71
MAM	8.79	18.97	8.09	17.68	9.34	12.17	20.88	4.01
Season	14.37	13.30	9.59	13.90	11.43	13.20	11.86	12.25

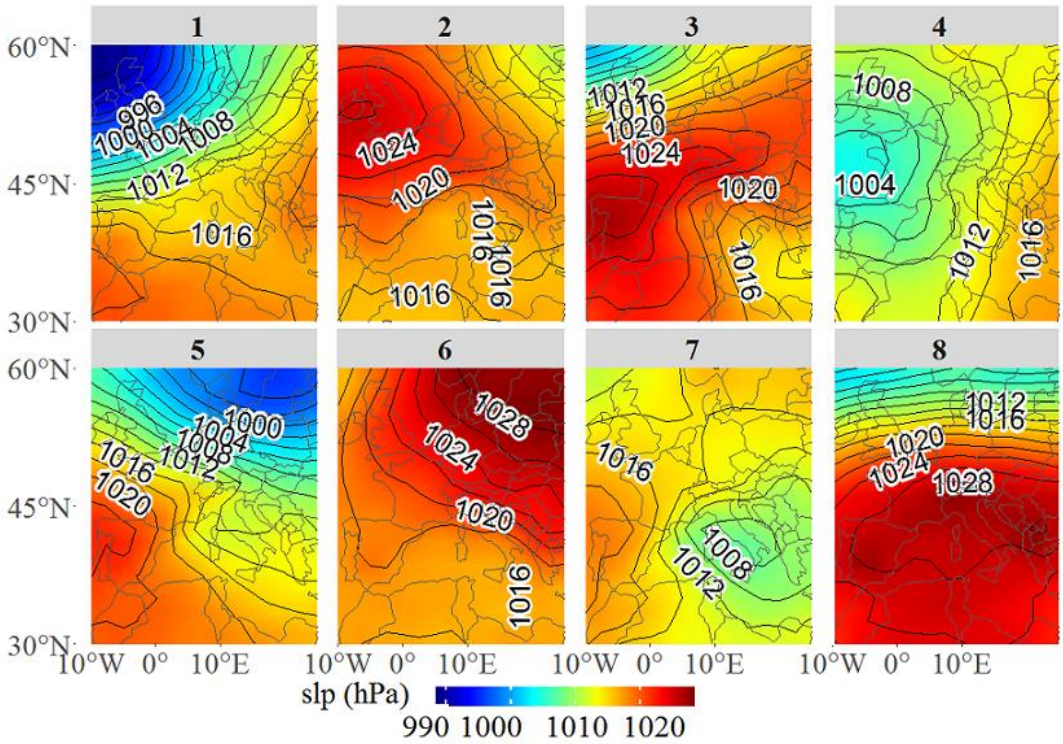

Figure 8. Spatial plot of the average sea level pressure at 500 hPa of each CT.

.TIFF size: 227.54 x 153.45 mm (300 x 300 DPI)

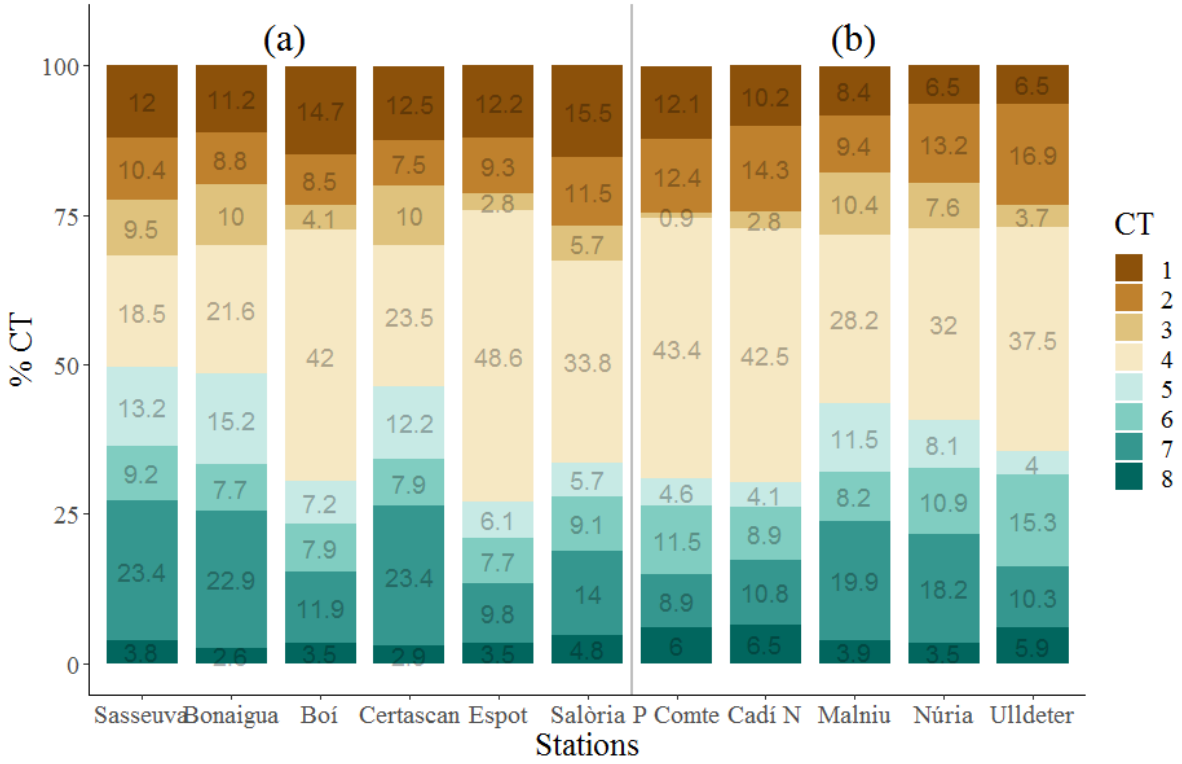

Figure 9. (a) Western Pyrenees and (b) eastern Pyrenees seasonal cumulative HN, classified by CT.

.TIFF size: 244.47 x 158.48 mm (300 x 300 DPI)

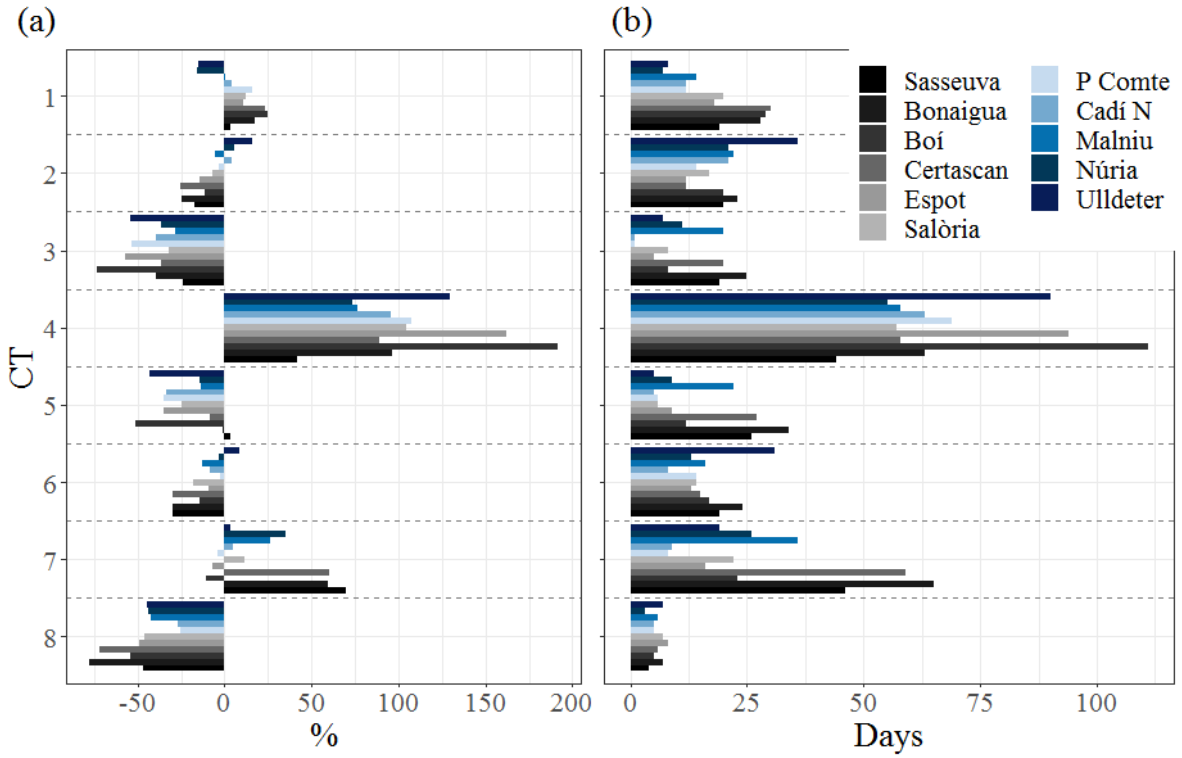

Figure 10. (a) Anomaly of HN days and (b) number of days with severe HN events (P>=75) grouped by CT and station. Anomalies were calculated by (i) sum all the snow days for each station, (ii) calculate the difference between the sum of the snow days grouped by CT and the total number of snow days and (iii) multiply for 100.

.TIFF size: 244.47 x 158.48 mm (300 x 300 DPI)

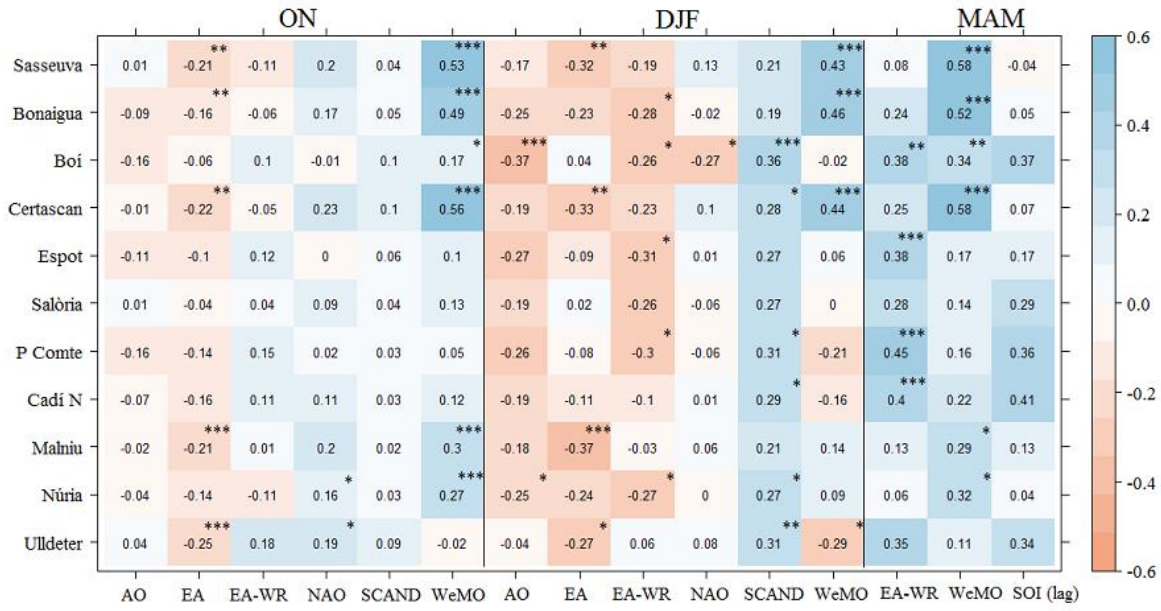

Figure 11. Pearson's correlation coefficients of the seasonal cumulative HN values and the teleconnection patterns that rule the study area, significant trends at *p <=0.05; **p <=0.01; ***p <=0.001.

.TIFF size: 241.30 x 127.26 mm (300 x 300 DPI)

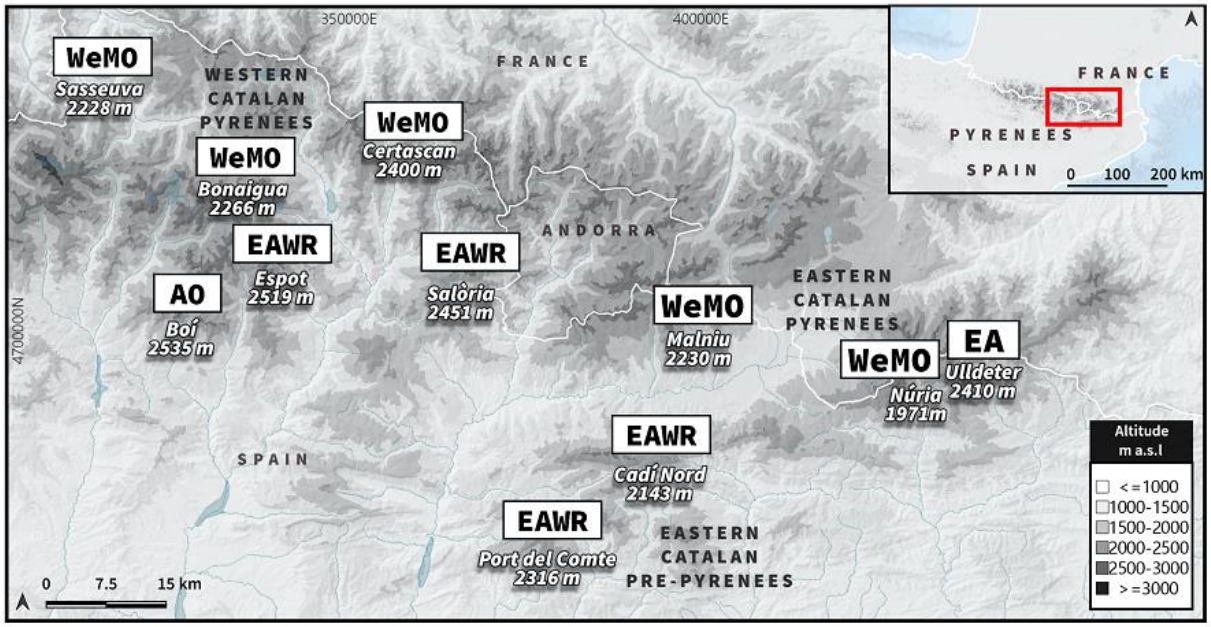

Figure 12. Spatial distribution of the teleconnection patterns that rule the study area. Data of the digital elevation model was downloaded from the European Environmental Agency (https://www.eea.europa.eu/data-and-maps/data/eu-dem).

.TIFF size: 234.68 x 122.50 mm (300 x 300 DPI)

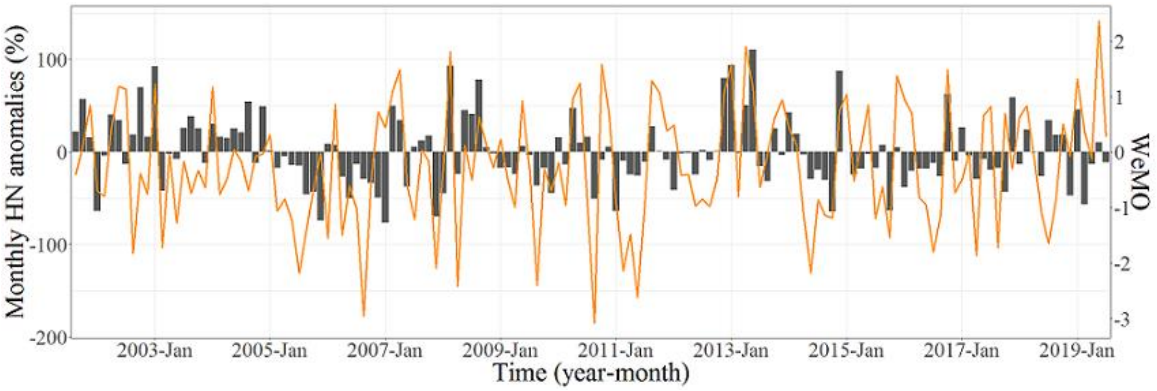

Figure 13. Anomaly graph between the average monthly HN values of the stations placed at the N western Catalan Pyrenees (Sasseuva, Bonaigua and Certascan; black bars) and the WeMO values (orange line).

.TIFF size: 225.16 x 75.14 mm (300 x 300 DPI)